SUPPLEMENTARY TEXT

A model of optimal protein allocation during phototrophic growth

Marjan Faizi, Tomáš Zavřel, Cristina Loureiro, Jan Červený, and Ralf Steuer

Contents

List of Figures

List of Tables

1 Model overview

We consider a coarse-grained model of proteome allocation in cyanobacteria to describe phototrophic growth. The model is described by ordinary differential equations (ODEs) and consists of the following processes and variables: uptake of external inorganic carbon (c_i^x) by a transporter protein T, conversion of the intracellular inorganic carbon pool (c_i) to amino acids (aa) by a metabolic multienzyme complex M, protein translation catalyzed by ribosomes R, and photosynthesis to produce energy units (e) that fuel all cellular processes. Energy production is implemented by activation of the photosystem unit (P^*) out of the inactivated state (P^0) due to light exposure. Energy production is restricted by product inhibition. In the extended version of the model external inorganic carbon c_i^x is also exchanged by passive diffusion and the activated photosynthetic unit P^* is subject to photodamage and degraded to amino acids. A schematic representation of the model is provided in figure 1 of the main text.

1.1 ODE System

The model is composed of 7 ODEs and one equation describing the growth rate. The ODEs are defined as follows

$$\frac{d[c_i]}{dt} = v_t - m_c \cdot v_m - \mu \cdot [c_i] \ ,$$

$$\frac{d[aa]}{dt} = v_m - \mu \cdot [aa] - \sum_j n_j \gamma_j \ ,$$

$$\frac{d[j]}{dt} = \gamma_j - \mu \cdot [j] \ ,$$

$$\frac{d[e]}{dt} = m_\phi \cdot v_2 - v_t - m_\mu \cdot v_m - \mu \cdot [e] - m_\gamma \cdot \sum_j n_j \gamma_j \ ,$$

and $\mu = \frac{1}{\mathcal{D}_c} \frac{v_t}{m_c}$.

$$v_t = [T] \cdot k_{cat}^t \cdot \frac{[c_i^x]}{K_t + [c_i^x]} \cdot \frac{[e]}{K_e + [e]}$$

$$v_m = [M] \cdot k_{cat}^m \cdot \frac{[c_i]}{K_m + [c_i]} \cdot \frac{[e]}{K_e + [e]}$$

$$\gamma_j = \beta_j \cdot \frac{\gamma_{\max}}{n_j} \cdot [R] \cdot \frac{[e]}{K_e + [e]} \cdot \frac{[aa]}{K_a + [aa]}$$

$$v_2 = \frac{k_2(e) \cdot \hat{\sigma} \cdot I \cdot [P]}{\hat{\sigma} \cdot I + k_2(e) + \mu}, \text{ with } k_2(e) = \frac{\tau}{1 + (\frac{[e]}{K_i})^4}$$

for j $\in \{\mathrm{R}, \mathrm{T}, \mathrm{M}, \mathrm{P}\}$

For the extended version of the model, including photodamage and diffusion, the following equations are modified

$$\frac{d[c_i]}{dt} = v_d + v_t - m_c \cdot v_m - \mu \cdot [c_i] \ ,$$

$$\frac{d[aa]}{dt} = v_m + n_P \cdot v_i - \mu \cdot [aa] - \sum_j n_j \gamma_j \ ,$$

$$\frac{d[P]}{dt} = \gamma_P - v_i - \mu \cdot [P] \ ,$$

and $\mu = \frac{1}{\mathcal{D}_c} \frac{v_t + v_d}{m_c}$.

$$v_d = P_m \cdot A_{cell} \cdot (N \cdot [c_i^x] - \frac{[c_i]}{V_{cell}})$$

$$v_i = \frac{k_d \cdot \hat{\sigma}^2 \cdot I^2 \cdot [P]}{\hat{\sigma} \cdot I + k_2(e) + k_d \cdot \hat{\sigma} \cdot I + \mu}$$

$$v_2 = \frac{k_2(e) \cdot \hat{\sigma} \cdot I \cdot [P]}{\hat{\sigma} \cdot I + k_2(e) + k_d \cdot \hat{\sigma} \cdot I + \mu}$$

All intracellular concentrations are indicated by units of molecules per cell. All parameters are listed in table 1 in the main text, and further descriptions are given in section 3. A more detailed description for the ODEs and the definition of the growth rate is provided in section 2.

1.2 Model assumptions

In order to keep the model as simple as possible, we make the following assumptions: (i) we neglect protein degradation, and at least for higher growth rates it is reasonable to assume that the dilution term is significantly higher than protein degradation; (ii) the energy unit e is a surrogate for all energy containing compounds (here ATP, GTP and NADPH), whereby we assume an interconversion ratio of 2.6 ATP $\widehat{=}$ 1 NADPH; (iii) we do not distinguish between CO_2 and HCO_3^- (or other forms of inorganic carbon); (iv) enzyme activity of RuBisCO is assumed to be the rate-limiting step during carbon metabolism; (v) half of the total cell mass is composed of proteins and only (approximately) half of the proteome is growth rate dependent; (vi) the cell volume and membrane surface are constant; (vii) photodamage affects the complete photosynthetic unit (as opposed to a repair cycle involving the D1 protein only).

2 Model description

2.1 Carbon metabolism

Carbon metabolism is represented by two steps: external inorganic carbon c_i^x is imported (v_t) into the cell by transporters T. Intracellular inorganic carbon c_i is then assimilated (v_m) into basic organic building blocks, here amino acids aa, that serve as precursor for protein synthesis. The synthesis of amino acids aa is catalyzed by a metabolic multienzyme complex M, which is composed of all enzymes that are required to catalyze the conversion from c_i to aa. We neglect an explicit CO_2 concentrating mechanism (CCM). We also do not distinguish between CO_2 or HCO_3^- and combine both as inorganic carbon c_i with the following dynamics

$$\frac{d[c_i]}{dt} = v_t - m_c \cdot v_m - \mu \cdot [c_i] \ , \tag{1}$$

with m_c denoting the number of c_i required to produce one amino acid. Both rates are described by Michaelis-Menten kinetics and depend on energy e

$$v_t = k_{\text{cat}}^t \cdot [T] \cdot \frac{[c_i^x]}{K_t + [c_i^x]} \cdot \frac{[e]}{K_e + [e]} \tag{2}$$

and

$$v_m = k_{\text{cat}}^m \cdot [M] \cdot \frac{[c_i]}{K_m + [c_i]} \cdot \frac{[e]}{K_e + [e]} \ , \tag{3}$$

where k_{cat}^t and k_{cat}^m are the maximal turnover rates of the transporter and metabolic enzyme, and K_t and K_m the corresponding half-saturation constants of both enzymes. The half-saturation constant K_e is, for simplicity, the same for all energy dependent reactions.

For the extended version of the model, we also considered nutrient uptake via diffusion. The amount of c_i^x that diffuses (v_d) through the cell depends on the permeability of the cell membrane P_m, the cell surface A_{cell} and the gradient of internal and external c_i

$$v_d = P_m \cdot A_{cell} \cdot (N_A \cdot [c_i^x] - \frac{[c_i]}{V_{cell}}) \ , \tag{4}$$

whereby V_{cell} and N_A are the cell volume and Avogadro constant, respectively, and are required to convert the units of c_i and c_i^x into numbers of molecules per liter, additionally A_{cell} and V_{cell} are, for simplicity, assumed to be constant. Hence, for the extended model the diffusion term v_d must be added to equation (1)

$$\frac{d[c_i]}{dt} = v_t + v_d - m_c \cdot v_m - \mu \cdot [c_i] \ . \tag{5}$$

2.2 Protein translation

Protein translation is modeled according to [1, 2]. Proteins are translated by ribosomes R, whereby amino acids aa serve as a precursor for protein synthesis and are produced (v_m) themselves out of inorganic carbon

$$\frac{d[aa]}{dt} = v_m - \mu \cdot [aa] - \sum_{j \in \{R,T,M,P\}} n_j \cdot \gamma_j \ , \tag{6}$$

where γ_j denotes the translation rate of protein complex j and n_j the size of the respective protein complex (in units of amino acids). In addition, translation depends here not only on availability of amino acids but also consumes energy. The translation rate γ_j for each protein complex j is described by

$$\gamma_j = \beta_j \cdot \frac{\gamma_{\max}}{n_j} \cdot [R] \cdot \frac{[e]}{K_e + [e]} \cdot \frac{[aa]}{K_a + [aa]} \ , \tag{7}$$

where $\gamma_{\max}$, denoting the maximal elongation rate, is divided by the size of the protein complex, since larger complexes take longer to translate. K_a indicates the half-saturation constant of ribosomes for amino acids and the factor β_j denotes the fraction of total ribosomes that are allocated to the translation of protein complex j and fulfills the constraint

$$\sum_{j \in \{R,T,M,P\}} \beta_j \leq 1 \ , \ \forall j : \beta_j \geq 0 \ . \tag{8}$$

The dynamics for the protein complexes R, T, and M are described by the equations

$$\frac{d[R]}{dt} = \gamma_R - \mu \cdot [R] \ , \tag{9}$$

$$\frac{d[T]}{dt} = \gamma_T - \mu \cdot [T] \ , \tag{10}$$

and

$$\frac{d[M]}{dt} = \gamma_M - \mu \cdot [M] \ . \tag{11}$$

2.3 Photosynthesis

The conversion of light into cellular energy is described by a minimal model of a photosynthetic unit, following the model of Han [3]. A photosynthetic unit is defined as an assembly of light-harvesting complexes (photosystem-I and -II) and an electron transport chain involved in the evolution of molecular oxygen [3]. The photosynthetic unit P exists in two states: inactivated P^0 and activated P^*. Light I facilitates the transition (v_1) to the activated state P^*, which then is involved in producing (v_2) energy e. The respective equations are

$$\frac{d[P^0]}{dt} = \gamma_P - v_1 + v_2 - \mu \cdot [P^0] \tag{12}$$

and

$$\frac{d[P^*]}{dt} = v_1 - v_2 - \mu \cdot [P^*] \ . \tag{13}$$

The fast transitions between both states of the photosynthetic unit are described by mass-action kinetics

$$v_1 = \hat{\sigma} \cdot I \cdot [P^0] \tag{14}$$

and

$$v_2 = k_2(e) \cdot [P^*] \ , \tag{15}$$

with

$$k_2(e) = \frac{\tau}{1 + (\frac{[e]}{Ki})^4} \tag{16}$$

where τ denotes the maximum turnover rate of the photosynthetic unit and $\hat{\sigma}$ the effective absorption cross-section, which determines the surface that is capable of absorbing a certain amount of photons. Additionally, v_2 contains a self-inhibition term for e, with an inhibition constant K_i, to regulate its own production, since energy production is not restricted by any other mechanism. Furthermore, we consider the dynamics of the concentration of the total photosynthetic unit to be $[P] = [P^0] + [P^*]$, so that

$$\frac{d[P]}{dt} = \gamma_P - \mu \underbrace{\left([P^0] + [P^*]\right)}_{[P]} \tag{17}$$

and assume a quasi-steady state for its activated form

$$\frac{d[P^*]}{dt} = 0 \iff [P^*] = \frac{\hat{\sigma} \cdot I \cdot [P]}{\hat{\sigma} \cdot I + k_2(e) + \mu} \ . \tag{18}$$

The rate of energy production is then $m_\phi \cdot v_2$, with m_ϕ determining the number of molecules produced per cycle, and

$$v_2 = k_2(e) \cdot [P^*] = \frac{k_2(e) \cdot \hat{\sigma} \cdot I \cdot [P]}{\hat{\sigma} \cdot I + k_2(e) + \mu} \ . \tag{19}$$

Thus, the energy balance with respect to e is given by the equation

$$\frac{d[e]}{dt} = m_\phi \cdot v_2 - v_\mathrm{t} - m_\mu \cdot v_\mathrm{m} - \mu \cdot [e] - m_\gamma \cdot \sum_{j \in \{R,T,M,P\}} n_j \cdot \gamma_j \ , \tag{20}$$

where m_μ and m_γ denote the number of e molecules required to produce one amino acid or for one translation elongation step, respectively. We note that the cellular component e combines

contributions from ATP, GTP and NADPH, and is assumed to have no carbon backbone but is only "recharged".

The coarse-grained model is extended with the capability to exhibit photoinhibition, which is a decline in the photosynthetic capacity and a result of high light intensities that damage the photosystem-II [4]. Applying this process to our model means that the photosynthetic unit can be damaged within the active state P^* and subsequently degraded to amino acids. The photoinhibition rate (v_i) is then calculated as follows (and happens at all light intensities proportional to the light intensity)

$$v_i = k_d \cdot \hat{\sigma} \cdot I \cdot [P^*] \ , \tag{21}$$

where k_d is the photodamge rate of the photosynthetic unit. Adding equation (21) to the definition of equation (18) yields

$$[P^*] = \frac{\hat{\sigma} \cdot I \cdot [P]}{\hat{\sigma} \cdot I + k_2(e) + k_d \cdot \hat{\sigma} \cdot I + \mu} \ , \tag{22}$$

and equation (17) is then modified to

$$\frac{d[P]}{dt} = \gamma_P - v_i - \mu \cdot [P] \ , \tag{23}$$

with

$$v_i = \frac{k_d \cdot \hat{\sigma}^2 \cdot I^2 \cdot [P]}{\hat{\sigma} \cdot I + k_2(e) + k_d \cdot \hat{\sigma} \cdot I + \mu} \ . \tag{24}$$

Furthermore, equation (6) gets an additional term, as the photosynthetic unit degrades back to amino acids

$$\frac{d[aa]}{dt} = v_m + n_P \cdot v_i - \mu \cdot [aa] - \sum_{j \in \{R,T,M,P\}} n_j \cdot \gamma_j \ . \tag{25}$$

2.4 Modeling bacterial growth

To study how the cell adapts its macromolecule composition on the basis of changing external conditions (I and c_i^x), we applied the ODE model to a nonlinear optimization problem. The optimization task is to find the proteome distribution, by adjusting the proportion of ribosomes β_j that are allocated to translate protein type j, that maximizes the (steady-state) growth rate (balanced growth). To simulate the ODE model, we use the parameters described below in section 3 (and are listed in table 1 of the main text). To ensure that the cell is forced to reallocate its proteome distribution for changing external conditions, the protein mass per cell volume is restricted to a fixed value and assumed to be approximately constant across different growth rates [5, 6]. Furthermore, we assume that the cell mass is proportional to the proteome mass, and therefore, define the total cell density $\mathcal{D}_c$ as weighted sum of all components in numbers of amino acids per cell (except for e which adds no weight to the mass)

$$\mathcal{D}_c = \frac{[c_i]}{m_c} + [aa] + \sum_{j \in \{R,T,M,P\}} n_j \cdot [j] \ , \tag{26}$$

thus, by applying the steady-state assumption, we obtain

$$\frac{d\mathcal{D}_c}{dt} = 0 \iff \frac{1}{m_c} \cdot \frac{d[c_i]}{dt} + \frac{d[aa]}{dt} + \sum_{j \in \{R,T,M,P\}} n_j \cdot \frac{d[j]}{dt} = 0 \ , \tag{27}$$

and after conversion

$$\mu \cdot \underbrace{(\frac{[c_i]}{m_c} + [aa] + \sum_{j \in \{R,T,M,P\}} n_j \cdot [j])}_{\mathcal{D}_c} = \frac{v_t}{m_c} \ . \tag{28}$$

Hence, the growth rate is defined as

$$\mu = \frac{v_t}{m_c \cdot \mathcal{D}_c} \ , \tag{29}$$

which serves as objective function for the optimization problem with respect to equation (8). Recalculating the growth rate for the extended model, including photoinhibition and diffusion, modifies equation (29) as follows

$$\mu = \frac{v_t + v_d}{m_c \cdot \mathcal{D}_c} \ . \tag{30}$$

3 Model Parameters

3.1 Stoichiometric coefficients

Carbon metabolism. The active transport of one external inorganic carbon via the bicarbonate transporter requires one ATP molecule. The production of one amino acid, with an average carbon chain length of $m_c = 5$, requires 17.9 ATP and 10.31 NADPH molecules, hence in total approximately $m_\mu = 45$ energy units (calculated using the metabolic network of Knoop et al. [7]).

Protein translation. We assume that each translational elongation step requires one ATP and two GTP molecules, which results in total in $m_\gamma = 3$ energy units (and one aa).

Photosynthesis. We further assume, based on the stoichiometric reconstruction [7], that each electron transport flow of the photosynthetic unit generates 2.6 ATP and 2 NAPDH molecules (normalized to the formation of one oxygen molecule), which equals to approximately $m_\phi = 8$ energy units.

3.2 Protein lengths

To determine the lengths for the four protein classes, we selected the model organism *Synechocystis sp.* PCC 6803 (hereafter called *Synechocystis*). The protein lengths of the ribosome, transporter and photosynthetic unit are determined using the UniProt database [8].

3.2.1 Ribosome R

All ribosomal protein subunits and their stoichiometry are listed in table T2 and T3. Each subunit appears once per ribosome, except for protein L7/L12, for which 4 copies are determined in *E.coli* [9], and both homologue proteins of S1 are counted as half. We do not take ribosomal RNA into account, since we only consider proteins for our cell mass. In total this sums up to a ribosome length of about 7358 amino acids.

3.2.2 Transporter T

The ATP-dependent bicarbonate transporter in *Synechocystis* represents our transporter enzyme (T) that facilitates c_i^x uptake and has a length of 1681 amino acids (see table T4).

3.2.3 Metabolic multienzyme complex M

We calculated the average amino acid length of a metabolic enzyme to be 345.77 with the genome-scale metabolic network of *Synechocystis* from Knoop et al. [7]. In addition, we calculated with this model the number of steps to convert inorganic carbon into an average amino acid, namely 82.8 steps. Thus, our metabolic multienzyme complex amounts to approximately 28630 amino acids.

3.2.4 Photosynthetic unit P

The photosynthetic unit is composed of all important proteins necessary for the photosynthetic electron flow [10], namely photosystem-I (PS–I) and -II (PS–II) including the light-harvesting complex phycobilisome, cytochrome b_6f, plastocyanin, ferredoxin-NADP$^+$ reductase (FNR) and ATP-synthase. According to the number of times the proteins are used to facilitate the transport of the electrons produced per formation of one oxygen molecule, the ratios within one photosynthetic unit are determined as follows: (i) 4· PS–I; (ii) 1· PS–II + phycobilisome; (iii) 2· cytochrome b_6f; (iv) 4· plastocyanin; (v) 4· FNR and (vi) $\frac{12}{14}$· ATP–synthase.
To determine the subunit stoichiometry of the phycobilisome, we follow the structural description of [11]. The PS–I complex exists in cyanobacteria in monomeric, dimeric and trimeric form [12], therefore we choose on average a dimeric form for PS–I. Additionally, the PS–II complex is accounted as a dimer. By considering the compositions of all proteins and their stoichiometry, listed in table T5-T9, this sums up to a protein length of approximately 95451 amino acids per photosynthetic unit.

3.3 Parameter estimation

Cell density. We assume that the cell density $\mathcal{D}_c$ is proportional to the proteome mass per cell volume. To calculate the proteome mass, we further assume that approximately half of the cell mass consists of proteins (following the biomass objective function used in Knoop et al. [7]). From the experimental measurements in table T1, we calculate the dry weight per cell and convert half of it into units of amino acids per cell. Additionally, we assume that there is a non-growth related proteome fraction of approximately 50% that does not contribute to growth [13]. Hence, the cell density $\mathcal{D}_c$ (in units of amino acids per cell volume), which is assumed to be proportional to the growth-related proteome mass per cell, is defined as follows

$$\mathcal{D}_c = 0.25 \cdot \frac{10^{-3} \cdot dry\ weight\ [\frac{mg}{L\ (culture)}]}{cell\ count\ [\frac{cells}{L\ (culture)}]} \cdot \frac{N}{100[\frac{Da}{aa}]} \quad , \tag{31}$$

where *dry weight* and *cell count* are the mean values taken from table T1. The results for each light intensity are plotted in figure S1. We therefore assume a value of $\mathcal{D}_c = 1.4{\cdot}10^{10}$ amino acids per cell.

Energy and amino acid threshold. The one-half-saturation constants for energy molecules during transport, metabolism and translation (K_e) and for amino acids (K_a) are chosen equal for simplicity and selected in such a way that they prevent energy and amino acid from becoming negative during the numerical computations.

Diffusion. The cell surface and volume (A_{cell} and V_{cell}) are required to convert the components of the diffusion term, hence to calculate them, we assume an average cell radius of 1.75 μm. To calculate the cell radius, we assume a constant dry weight per cell of 8.67 pg (average of all dry weight values in table T1). Assuming further that the dry mass per volume is $0.3-0.5$ pg/μm^3 [14], leads to a cell volume of $17.35 - 28.91$ μm^3 and consequently also to a cell radius of $1.6 - 1.9$ μm. Furthermore, we assume that the permeability of c_i^x corresponds to the permeability of bicarbonate molecules HCO_3^- [15], since most of the inorganic carbon at least in seawater is in the form of HCO_3^- and dissolved CO_2 represents only a small fraction of less than 1% [16].

Photosynthesis. To determine the remaining parameters of the photosynthetic part of the model (τ, $\hat{\sigma}$ and k_d), we set the external inorganic carbon concentration to a fixed value $[c_i^x] = 1000$ μM (2000 μM is observed in seawater [17]), however, we assume a lower concentration in the medium because of the higher density of cells compared to seawater conditions). We estimate the parameters by fitting the model to the experimental data given in table T1. In order to get a better sense of what order of magnitude the parameters are, we followed the model of Han [18], where the photodamage kd ranges between $0 - 10^{-7}$, the effective absorption cross-section $\hat{\sigma}$ between $0.6 - 3.0$ $m^2/\mu E$ and the turnover rate of the photosynthetic unit τ between $1000 - 10000$ s^{-1}. However, those parameter ranges are too high for our model, meaning that the resulting growth curve is far above the experimental measurements. Therefore, we chose different boundaries for our parameters and figure S2 shows the range of possible growth curves that can be simulated with the following ranges

$$\hat{\sigma} = 0.1 - 0.3\ [\tfrac{m^2}{\mu E}]\ , \quad k_d = 10^{-6} - 5 \cdot 10^{-6} \quad \text{and} \quad \tau = 1000 - 4000\ [min^{-1}].$$

In this region we searched for those parameters $\hat{\sigma}$, k_d and τ that minimize the distance between experimental and simulated growth rates. Therefore we minimize the negative logarithm of the likelihood $l(\theta)$ as follows

$$l(\theta) = \sum_i [(\frac{y_i(\theta) - x_i}{\sigma_i})^2 + log(2\pi\sigma_i^2)]\ , \tag{32}$$

where x_i represents the experimental data with their uncertainties σ_i and $y(\theta)_i$ denotes the simulated data points calculated with the model parameters θ. Figure S2 shows the best fit with $l(\theta) = -61.43$, obtained with the parameters: $\tau = 1900\ [min^{-1}]$, $\hat{\sigma} = 0.166\ [\frac{m^2}{\mu E}]$ and $k_d = 1.6{\cdot}10^{-6}$.

Subsequently, we compared the oxygen evolution rate with the energy production rate v_2, to test the model performance. The oxygen evolution rate v_{O_2} is defined as the difference between photosynthesis v_{photo} and respiration rate v_{resp} (see table T1). The energy production rate v_2 is

described in units of molecules per cell per time, while the oxygen evolution rate v_{O_2} is normalized to the amount of dry weight

$$v_{O_2}[\mu mol(O_2)\ mg^{-1}s^{-1}] = (v_{photo} - v_{resp}) \cdot \frac{10^{-3} \cdot chlorophyll\ a}{dry\ weight} \quad . \tag{33}$$

4 Supplementary Figures and Tables

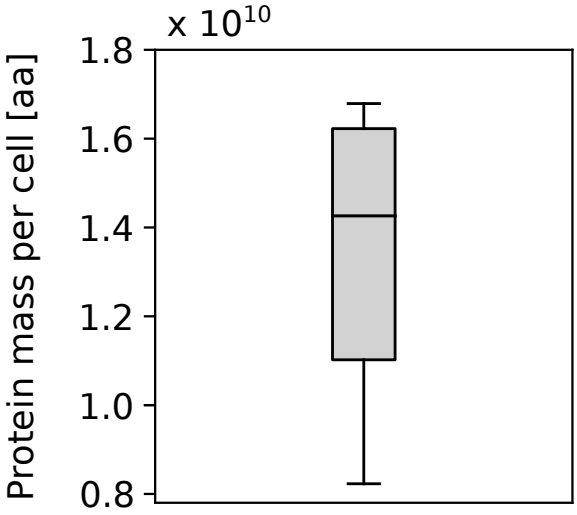

Figure S1: Estimation of protein mass. We calculated the total protein mass as 50% of the dry weight per cell and converted it into units of amino acids (aa). Additionally, we assume that 50% of the proteome does not contribute to growth. The total protein mass is plotted for each light intensity from Table T1, whereby we only considered the mean values. The median is around $1.4 \cdot 10^{10}$ [aa per cell].

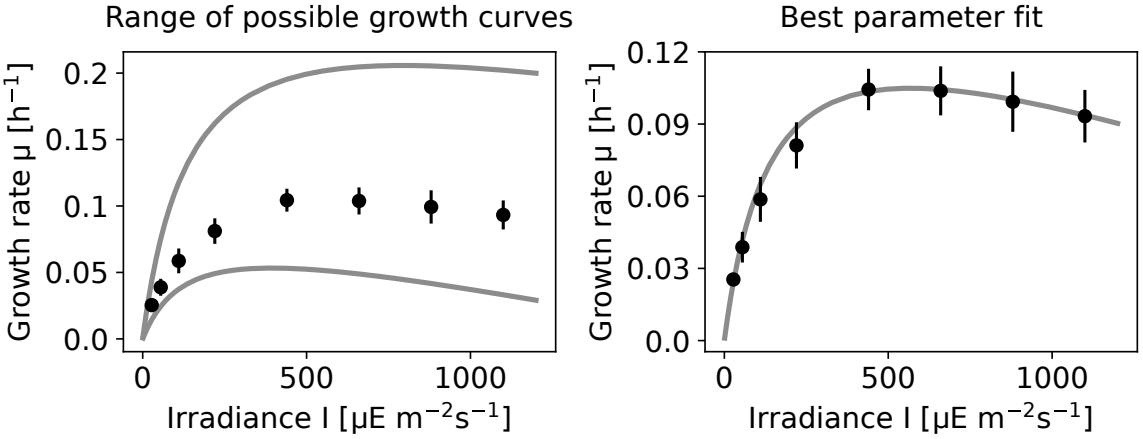

Figure S2: Parameter fitting of the photosynthetic part. Experimental data (black circle) in comparison to simulated growth curves (solid gray line) with different parameter sets for the turnover rate of the photosystem (τ), photodamage rate (k_d) and effective absorption cross-section ($\hat{\sigma}$). The left plot shows the range of growth curves that can be simulated within the parameter boundaries. The lower left curve is simulated with $\tau = 1000$, $k_d = 2.5 \cdot 10^{-6}$ and $\hat{\sigma} = 0.1$, while the upper growth curve is simulated with $\tau = 4000$, $k_d = 10^{-6}$ and $\hat{\sigma} = 0.3$. The best fit on the right plot is obtained with $\tau = 1900$, $k_d = 1.6 \cdot 10^{-6}$ and $\hat{\sigma} = 0.166$. All model simulations are performed with $c_i^x = 1000$ μM.

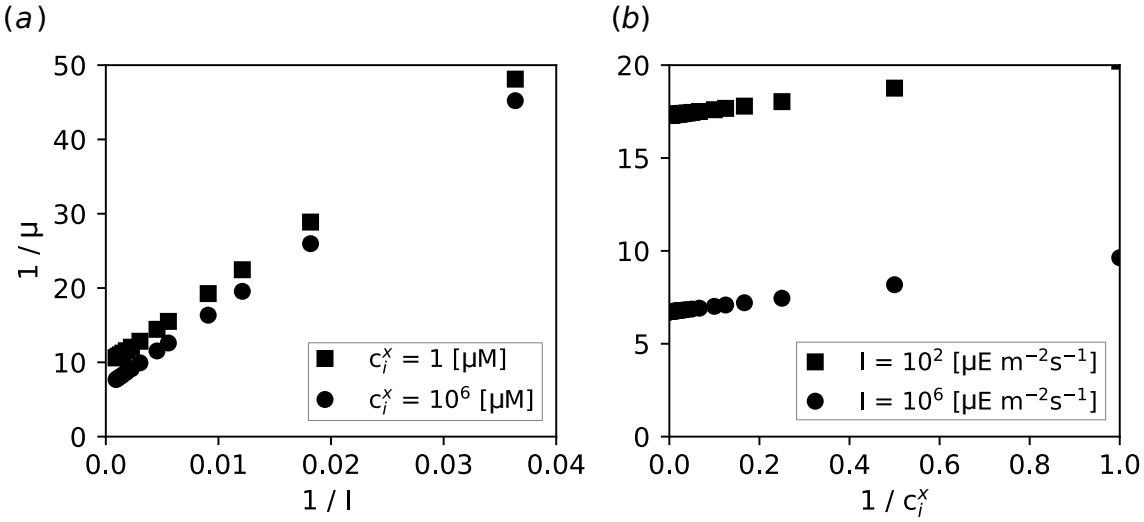

Figure S3: Lineweaver-Burk plot. A Lineweaver–Burk (LB) plot is a double reciprocal plot of growth rate versus light intensity and carbon availability. Parallel lines in the LB plot are characteristic for uncompetitive inhibition (limitation by external inorganic carbon or light acts as an uncompetitive inhibitor and lowers the apparent K_m and V_m values for the other nutrient). μ: growth rate [h^{-1}], I: Irradiance [μE $m^{-2}s^{-1}$] and c_i^x: external inorganic carbon [μM].

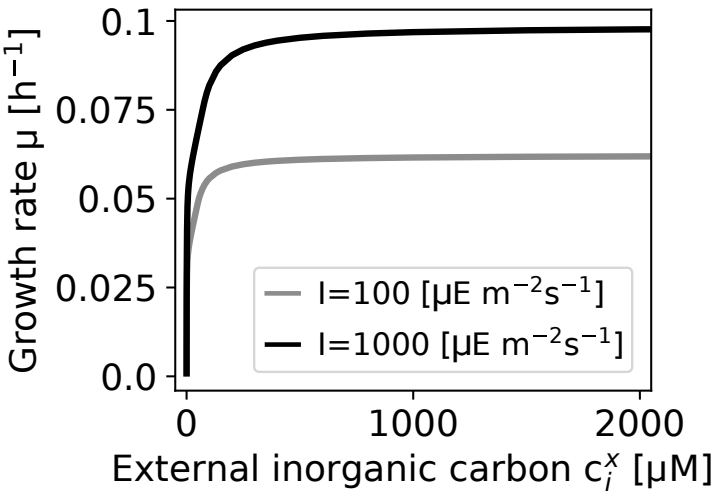

Figure S4: Growth as a function of c_i^x in the extended model. Growth rates are simulated for two different light intensities (I). Due to the diffusion term in the extended model the growth curve for increasing c_i^x does not follow a Monod-like shape.

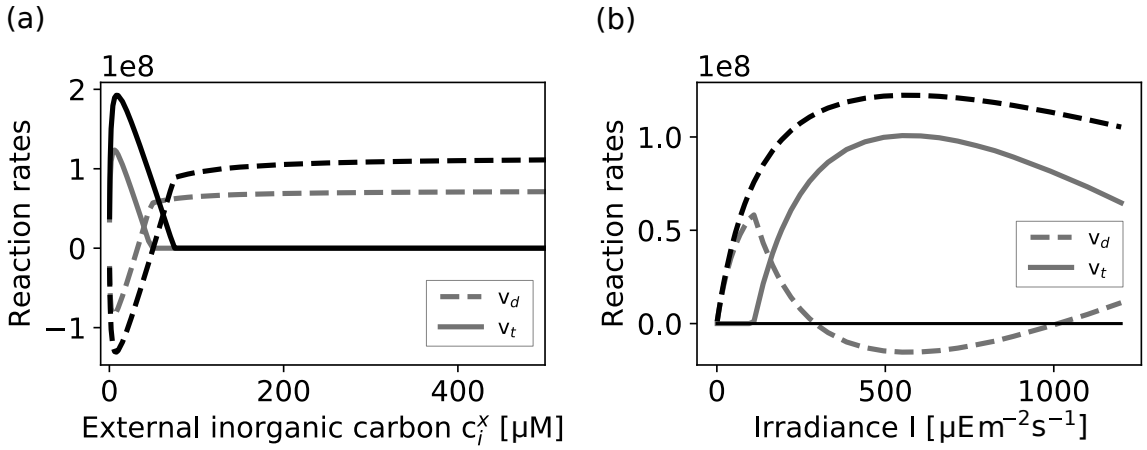

Figure S5: Carbon uptake rates. Shown is active carbon transport rate (v_t, solid line) and the diffusion rate (v_d, dashed line) for different external conditions. **(a)** Reaction rates for increasing external inorganic carbon c_i^x and two (constant) light intensities, $I = 100$ μE m^{-2}s^{-1} (gray curve) and $I = 1000$ μE m^{-2}s^{-1} (black curve), respectively. For low external carbon, carbon uptake is facilitated by active transport, whereas passive diffusion results in a net loss of inorganic carbon (carbon cycling). As the concentration of external inorganic carbon increases, the required activity of the transport decreases. At some point, the direction of diffusion changes sign and results in a net import of inorganic carbon into the cell. For high external inorganic carbon, the transport is not expressed. **(b)** Reaction rates for increasing light intensity I and two (fixed) concentrations of c_i^x, $c_i^x = 50$ μM (gray curve) and $c_i^x = 1000$ μM (black curve), respectively. For low light (and hence slow growth), the demand for inorganic carbon is met by passive diffusion. For a critical light intensity, and low inorganic carbon (gray line), active transport is induced.

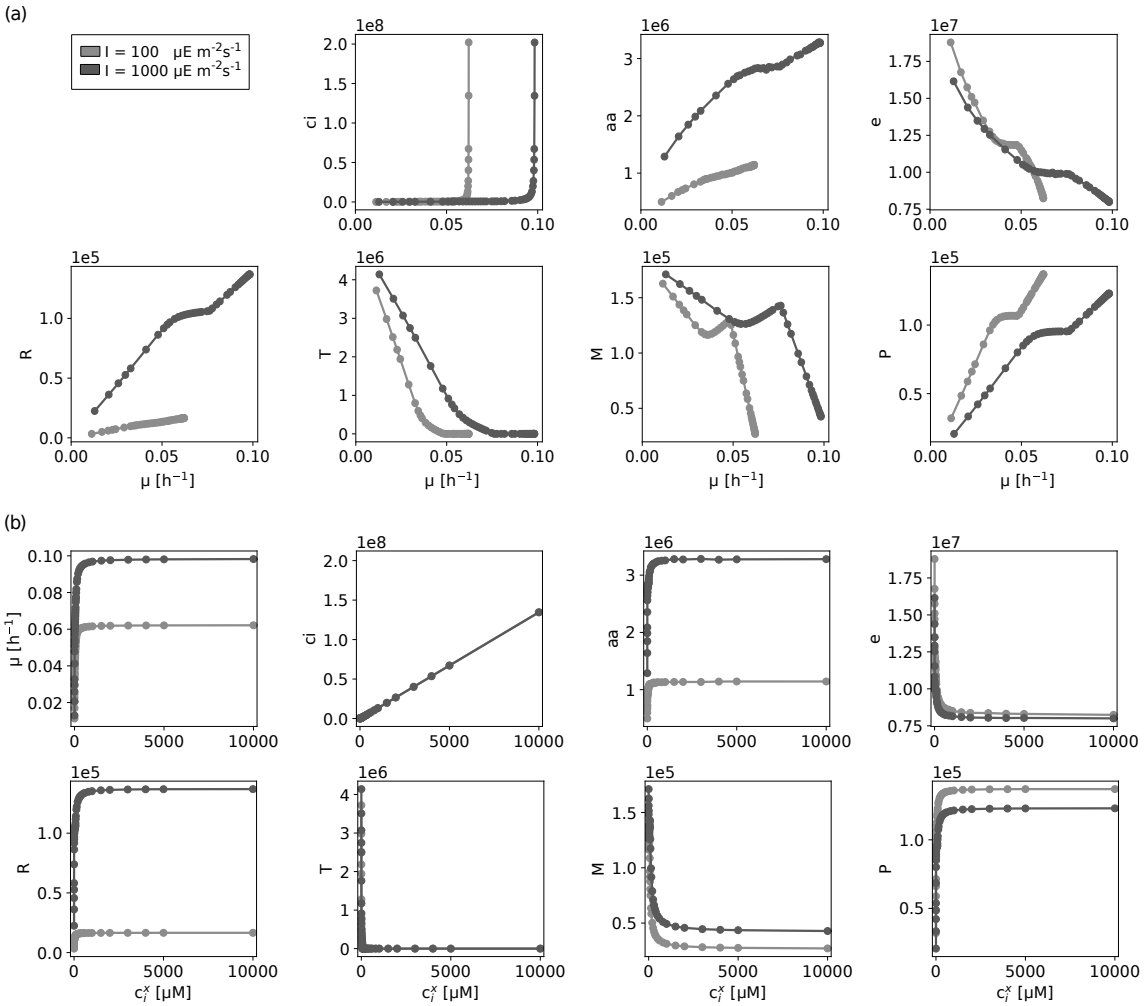

Figure S6: Concentrations of intracellular compounds for increasing c_i^x (extended model). Molecules per cell are displayed (a) as a function of growth rate μ, and (b) as a function of external inorganic carbon c_i^x for two different light conditions. ci: inorganic carbon; aa: amino acid; e: energy unit; R: ribosome; T: transporter; M: metabolic enzyme; P: photosynthetic unit.

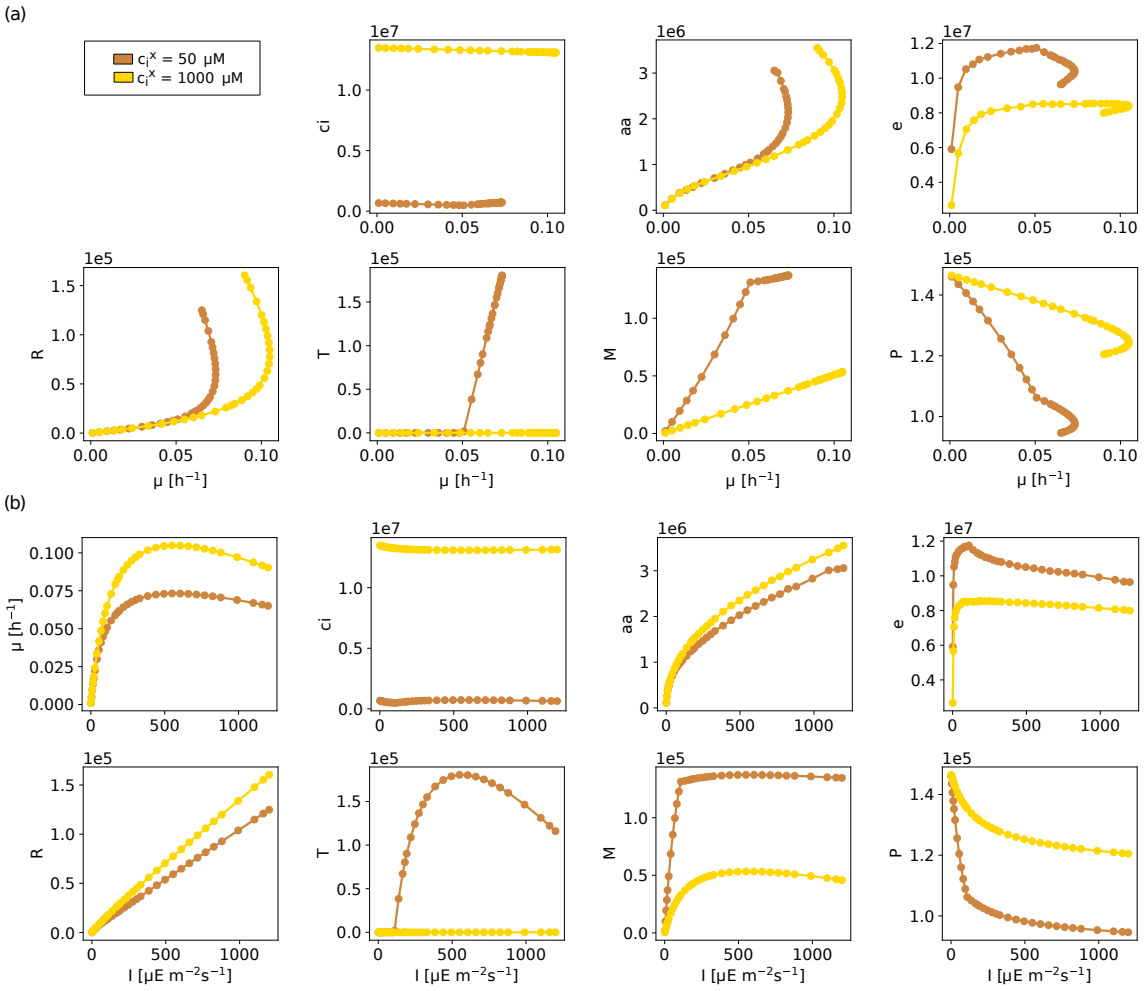

Figure S7: Concentrations of intracellular compounds for increasing I (extended model). Molecules per cell are displayed (a) as a function of growth rate μ (b), as a function of light intensity I for two different c_i^x concentrations in both panels. Notably, the mass-fraction of ribosomes increase linearly as a function of light intensity. ci: inorganic carbon; aa: amino acid; e: energy unit; R: ribosome; T: transporter; M: metabolic enzyme; P: photosynthetic unit.

Table T1: Data obtained for *Synechocystis* 6803 sub-strain (GT-L) using controlled turbidostat experiments.

red light [μE $m^{-2}s^{-1}$]		27.5	55	110	220
specific growth rate [h^{-1}]	mean	0.02540	0.03882	0.05869	0.08112
	sd	0.00178	0.00637	0.00933	0.00961
chlorophyll (a) [μmol L(culture)$^{-1}$]	mean	2.36657	2.53722	2.22747	2.26997
	sd	0.28530	0.22823	0.21533	0.22739
dry weight [mg L(culture)$^{-1}$]	mean	132.200	165.583	173.000	219.562
	sd	39.7816	58.4965	29.0517	50.1615
cell count [cells L(culture)$^{-1}$]	mean	2.52E10	2.54E10	2.14E10	2.10E10
	sd	2.98E09	3.31E09	4.94E09	2.11E09
photosynthesis [μmol(O_2) mmol(Chl)$^{-1}s^{-1}$]	mean	30.4787	42.5266	80.6806	119.475
	sd	5.65365	6.90414	11.7693	19.0497
respiration [μmol(O_2) mmol(Chl)$^{-1}s^{-1}$]	mean	-5.45712	-6.43310	-12.3565	-18.9473
	sd	2.70102	1.11482	5.97641	2.29437

red light [μE $m^{-2}s^{-1}$]		440	660	880	1100
specific growth rate [h^{-1}]	mean	0.10436	0.10380	0.09928	0.09327
	sd	0.00862	0.01019	0.01252	0.01092
chlorophyll (a) [μmol L(culture)$^{-1}$]	mean	1.93189	1.88480	1.67495	1.49722
	sd	0.05443	0.18380	0.13364	0.15200
dry weight [mg L(culture)$^{-1}$]	mean	221.375	259.750	256.375	230.857
	sd	15.1183	19.2635	21.5460	58.6158
cell count [cells L(culture)$^{-1}$]	mean	2.56E10	2.30E10	2.43E10	2.68E10
	sd	2.02E09	4.45E09	4.30E09	4.46E09
photosynthesis [μmol(O_2) mmol(Chl)$^{-1}s^{-1}$]	mean	184.629		251.599	
	sd	24.7217		49.4417	
respiration [μmol(O_2) mmol(Chl)$^{-1}s^{-1}$]	mean	-24.6819		-40.9372	
	sd	7.61381		14.6008	

Table T2: Ribosomal proteins in *Synechocystis* 6803 (large subunits).

Uniprot ID	Gene name	Protein name	Stoichiometry	Length
P36236	rplA	50S ribosomal protein L1	1	238
P73317	rplB	50S ribosomal protein L2	1	276
P73320	rplC	50S ribosomal protein L3	1	213
P73319	rplD	50S ribosomal protein L4	1	210
P73308	rplE	50S ribosomal protein L5	1	180
P73306	rplF	50S ribosomal protein L6	1	179
P42352	rplI	50S ribosomal protein L9	1	152
P23350	rplJ	50S ribosomal protein L10	1	173
P36237	rplK	50S ribosomal protein L11	1	141
P23349	rplL	50S ribosomal protein L7/L12	4	128
P73294	rplM	50S ribosomal protein L13	1	151
P73310	rplN	50S ribosomal protein L14	1	122
P73303	rplO	50S ribosomal protein L15	1	147
P73313	rplP	50S ribosomal protein L16	1	139
P73296	rplQ	50S ribosomal protein L17	1	116
P73305	rplR	50S ribosomal protein L18	1	120
P36239	rplS	50S ribosomal protein L19	1	122
P48957	rplT	50S ribosomal protein L20	1	117
P74266	rplU	50S ribosomal protein L21	1	124
P73315	rplV	50S ribosomal protein L22	1	121
P73318	rplW	50S ribosomal protein L23	1	101
P73309	rplX	50S ribosomal protein L24	1	115
P73289	rplY	50S ribosomal protein L25	1	98
P74267	rpmA	50S ribosomal protein L27	1	87
P72851	rpmB	50S ribosomal protein L28	1	78
P73312	rpmC	50S ribosomal protein L29	1	73
P73292	rpmE	50S ribosomal protein L31	1	81
P73014	rpmF	50S ribosomal protein L32	1	57
P48958	rpmG	50S ribosomal protein L33	1	65
Q55004	rpmH	50S ribosomal protein L34	1	45
P48959	rpmI	50S ribosomal protein L35	1	67
P73300	rpmJ	50S ribosomal protein L36	1	38
Total				4458

Table T3: Ribosomal proteins in *Synechocystis* 6803 (small subunits).

Uniprot ID	Gene name	Protein name	Stoichiometry	Length
P73530	rps1A	30S ribosomal protein S1 homolog A	0.5	328
P74142	rps1b	30S ribosomal protein S1 homolog B	0.5	305
P74071	rpsB	30S ribosomal protein S2	1	269
P73314	rpsC	30S ribosomal protein S3	1	240
P48939	rpsD	30S ribosomal protein S4	1	202
P73304	rpsE	30S ribosomal protein S5	1	173
P73636	rpsF	30S ribosomal protein S6	1	113
P74229	rpsG	30S ribosomal protein S7	1	156
P73307	rpsH	30S ribosomal protein S8	1	133
P73293	rpsI	30S ribosomal protein S9	1	137
P74226	rpsJ	30S ribosomal protein S10	1	105
P73298	rpsK	30S ribosomal protein S11	1	130
P74230	rpsL	30S ribosomal protein S12	1	126
P73299	rpsM	30S ribosomal protein S13	1	127
P48944	rpsN	30S ribosomal protein S14	1	100
P72866	rpsO	30S ribosomal protein S15	1	89
P74410	rpsP	30S ribosomal protein S16	1	82
P73311	rpsQ	30S ribosomal protein S17	1	81
P48946	rpsR	30S ribosomal protein S18	1	71
P73316	rpsS	30S ribosomal protein S19	1	92
P73336	rpsT	30S ribosomal protein S20	1	97
P48949	rpsU	30S ribosomal protein S21	1	60
Total				2899.5

Table T4: Bicarbonate transporter in *Synechocystis* 6803.

Uniprot ID	Gene name	Protein name	Stoichiometry	Length
Q55460	cmpA	Bicarbonate-binding protein CmpA	1	452
Q55461	cmpB	Bicarbonate transport system permease protein CmpB	1	280
Q55462	cmpC	Bicarbonate transport ATP-binding protein CmpC	1	667
Q55463	cmpD	Bicarbonate transport ATP-binding protein CmpD	1	282
Total				1681

Table T5: Photosystem-I monomer in *Synechocystis* 6803.

Uniprot ID	Gene name	Protein name	Stoichiometry	Length
P29254	psaA	Photosystem I P700 chlorophyll a apoprotein A1 (PsaA)	1	751
P29255	psaB	Photosystem I P700 chlorophyll a apoprotein A2 (PsaB)	1	731
P32422	psaC	Photosystem I iron-sulfur center (Photosystem I subunit VII) (PsaC)	1	81
P19569	psaD	Photosystem I reaction center subunit II (PSI-D)	1	141
P12975	psaE	Photosystem I reaction center subunit IV (p30 protein)	1	74
P29256	psaF	Photosystem I reaction center subunit III (PSI-F)	1	165
Q55330	psaI	Photosystem I reaction center subunit VIII	1	40
Q55329	psaJ	Photosystem I reaction center subunit IX	1	40
P72712	psaK1	Photosystem I reaction center subunit PsaK 1 (Photosystem I subunit X 1)	1	86
P74564	psaK2	Photosystem I reaction center subunit PsaK 2 (Photosystem I subunit X 2)	1	90
P37277	psaL	Photosystem I reaction center subunit XI (PSI-L)	1	157
P72986	psaM	Photosystem I reaction center subunit XII (PSI-M)	1	31
Total				2387

Table T6: Photosystem-II monomer in *Synechocystis* 6803.

Uniprot ID	Gene name	Protein name	Stoichiometry	Length
P74367	psb27	Photosystem II lipoprotein Psb27	1	134
Q55356	psb28	Photosystem II reaction center Psb28 protein (Photosystem II reaction center W protein)	1	112
P07826	psbA1	Photosystem II protein D1 1 (PSII D1 protein 1) (Photosystem II Q(B) protein 1)	1	360
P16033	psbA2	Photosystem II protein D1 2 (PSII D1 protein 2) (Photosystem II Q(B) protein 2)	1	360
P05429	psbB	Photosystem II CP47 reaction center protein (Protein CP-47)	1	507
P09193	psbC	Photosystem II CP43 reaction center protein (Protein CP-43)	1	460
P09192	psbD	Photosystem II D2 protein (PSII D2 protein) (Photosystem Q(A) protein)	1	352
P09190	psbE	Cytochrome b559 subunit alpha (PSII reaction center subunit V)	1	81
P09191	psbF	Cytochrome b559 subunit beta (PSII reaction center subunit VI)	1	44
P14835	psbH	Photosystem II reaction center protein H (PSII-H)	1	64
Q54697	psbI	Photosystem II reaction center protein I (PSII-I)	1	38
P73070	psbJ	Photosystem II reaction center protein J (PSII-J)	1	39
P15819	psbK	Photosystem II reaction center protein K (PSII-K)	1	45
Q55354	psbL	Photosystem II reaction center protein L (PSII-L)	1	39
P72701	psbM	Photosystem II reaction center protein M (PSII-M)	1	35
P26286	psbN	Protein PsbN	1	43
P10549	psbO	Photosystem II manganese-stabilizing polypeptide (MSP)	1	274
P74787	psbT	Photosystem II reaction center protein T (PSII-T)	1	31
Q55332	psbU	Photosystem II 12 kDa extrinsic protein (PS II complex 12 kDa extrinsic protein) (PSII-U)	1	131
Q55013	psbV	Cytochrome c-550 (Cytochrome c549) (Cytochrome c550) (Low-potential cytochrome c)	1	160
P72575	psbX	Photosystem II reaction center X protein	1	39
P73676	psbY	Photosystem II protein Y	1	39
P73528	psbZ	Photosystem II reaction center protein Z (PSII-Z)	1	62
Q55438	ycf12	Photosystem II reaction center protein Ycf12	1	39
Total				3488

Table T7: Cytochrome b_6f homodimer, plastocyanin and FNR in *Synechocystis* 6803.

Uniprot ID	Gene name	Protein name	Stoichiometry	Length
P26287	petA	Cytochrome f	2	328
Q57038	petB	Cytochrome b6	2	222
P74714	petC1	Cytochrome b6-f complex iron-sulfur subunit 1 (Rieske iron-sulfur protein 1)	2	178
P27589	petD	Cytochrome b6-f complex subunit 4	2	160
P74149	petG	Cytochrome b6-f complex subunit 5	2	38
P74810	petM	Cytochrome b6-f complex subunit 7	2	36
P72717	petN	Cytochrome b6-f complex subunit 8	2	29
Total				1982
P21697	petE	Plastocyanin	1	126
Q55318	petH	Ferredoxin–NADP reductase (FNR)	1	413

Table T8: ATP-synthase in *Synechocystis* 6803.

Uniprot ID	Gene name	Protein name	Stoichiometry	Length
P27179	atpA	ATP synthase subunit alpha (ATP synthase F1 sector subunit alpha)	3	503
P27178	atpB	ATP synthase subunit a (ATP synthase F0 sector subunit a)	1	276
P26533	atpC	ATP synthase epsilon chain (ATP synthase F1 sector epsilon subunit)	1	136
P26527	atpD	ATP synthase subunit beta (ATP synthase F1 sector subunit beta)	3	483
P27182	atpE	ATP synthase subunit c (ATP synthase F(0) sector subunit c)	10-14	81
P27181	atpF	ATP synthase subunit b (ATP synthase F(0) sector subunit b)	1	179
P17253	atpG	ATP synthase gamma chain (ATP synthase F1 sector gamma subunit)	1	314
P27183	atpG	ATP synthase subunit b' (ATP synthase F(0) sector subunit b')	1	143
P27180	atpH	ATP synthase subunit delta (ATP synthase F(1) sector subunit delta)	1	185
On average				5163

Table T9: Phycobilisome in *Synechocystis* 6803.

Uniprot ID	Gene name	Protein name	Stoichiometry	Length
		3-cylindric core each with 4 trimeric allophycocyanin $(\alpha\beta)_3$ discs		
Q01951	apcA	Allophycocyanin alpha chain	34	161
Q01952	apcB	Allophycocyanin beta chain	34	161
Q01950	apcC	Phycobilisome linker polypeptide, allophycocyanin-associated, core (LC 7.8)	6	67
P72870	apcD	Allophycocyanin subunit alpha-B	2	161
Q55544	apcE	Phycobiliprotein ApcE (Phycobilisome LCM core-membrane linker polypeptide)	6	896
P74551	apcF	Allophycocyanin subunit beta-18	2	169
		6 rods each with 3 hexameric phycocyanin $(\alpha\beta)_6$ discs		
Q54715	cpcA	C-phycocyanin alpha chain	108	162
Q54714	cpcB	C-phycocyanin beta chain	108	172
P73203	cpcC1	Phycobilisome linker polypeptide, phycocyanin-associated, rod 1	6	291
P73204	cpcC2	Phycobilisome linker polypeptide, phycocyanin-associated, rod 2	6	273
P73202	cpcD	Phycobilisome linker polypeptide, phycocyanin-associated, rod (L-8.9/R) (Rod-capping linker protein)	6	83
P74625	cpcG	Phycobilisome rod-core linker polypeptide CpcG	6	249
Total				58834

References

[1] Douwe Molenaar, Rogier van Berlo, Dick de Ridder, and Bas Teusink. Shifts in growth strategies reflect tradeoffs in cellular economics. *Mol. Syst. Biol.*, 5:323, 2009.

[2] Arijit Maitra and Ken A Dill. Bacterial growth laws reflect the evolutionary importance of energy efficiency. *Proc. Natl. Acad. Sci. U.S.A.*, 112(2):406–411, 2015.

[3] Bo-Ping Han. Photosynthesis–irradiance response at physiological level: a mechanistic model. *J. Theor. Biol.*, 213(2):121–127, 2001.

[4] Bo-Ping Han. A mechanistic model of algal photoinhibition induced by photodamage to photosystem-ii. *J. Theor. Biol.*, 214(4):519–527, 2002.

[5] Hans Bremer and Patrick P Dennis. Modulation of chemical composition and other parameters of the cell at different exponential growth rates. *EcoSal Plus*, 3(1), 2008.

[6] Andrea Y. Weiße, Diego A. Oyarzún, Vincent Danos, and Peter S. Swain. Mechanistic links between cellular trade-offs, gene expression, and growth. *Proc. Natl. Acad. Sci. U.S.A.*, 112(9):E1038–47, 2015.

[7] Henning Knoop, Marianne Gründel, Yvonne Zilliges, Robert Lehmann, Sabrina Hoffmann, Wolfgang Lockau, and Ralf Steuer. Flux balance analysis of cyanobacterial metabolism: The metabolic network of Synechocystis sp. PCC 6803. *PLoS Comput. Biol.*, 9(6):e1003081, 2013.

[8] UniProt Consortium. UniProt: the universal protein knowledgebase. *Nucleic Acids Res.*, 45(D1):D158–D169, 2017.

[9] Alap Raman Subramanian. Copies of proteins L7 and L12 and heterogeneity of the large subunit of Escherichia coli ribosome. *J. Mol. Biol.*, 95(1):1–4, 1975.

[10] Wim FJ Vermaas. Photosynthesis and respiration in cyanobacteria. *eLS*, 2001.

[11] Ana A Arteni, Ghada Ajlani, and Egbert J Boekema. Structural organisation of phycobilisomes from synechocystis sp. strain PCC6803 and their interaction with the membrane. *Biochim. Biophys. Acta*, 1787(4):272–279, 2009.

[12] Hisako Kubota, Isamu Sakurai, Kenta Katayama, Naoki Mizusawa, Shunsuke Ohashi, Masami Kobayashi, Pengpeng Zhang, Eva-Mari Aro, and Hajime Wada. Purification and characterization of photosystem i complex from Synechocystis sp. PCC 6803 by expressing histidine-tagged subunits. *Biochim. Biophys. Acta, Bioenerg.*, 1797(1):98–105, 2010.

[13] Alexandra-M. Reimers, Henning Knoop, Alexander Bockmayr, and Ralf Steuer. Cellular trade-offs and optimal resource allocation during cyanobacterial diurnal growth. *Proc. Natl. Acad. Sci. U.S.A.*, 114(31):E6457–E6465, 2017.

[14] Ron Milo and Rob Phillips. *Cell biology by the numbers*. Taylor & Francis Ltd., 2015.

[15] Niall M Mangan and Michael P Brenner. Systems analysis of the CO2 concentrating mechanism in cyanobacteria. *eLife*, 3:e02043, 2014.

[16] Elena V Kupriyanova, Maria A Sinetova, Sung Mi Cho, Youn-Il Park, Dmitry A Los, and Natalia A Pronina. CO2-concentrating mechanism in cyanobacterial photosynthesis: organization, physiological role, and evolutionary origin. *Photosynth. Res.*, 117(1):133–146, 2013.

[17] Brian M Hopkinson, Jodi N Young, Anna L Tansik, and Brian J Binder. The minimal CO2-concentrating mechanism of Prochlorococcus spp. MED4 is effective and efficient. *Plant Physiol.*, 166(4):2205–2217, December 2014.

[18] Bo-Ping Han, Markku Virtanen, Jorma Koponen, and Milan Straskraba. Effect of photoinhibition on algal photosynthesis: a dynamic model. *J. Plankton Res.*, 22(5):865–885, 2000.